

One-to-one spatially matched experiment and atomistic simulations of nanometre-scale indentation

This content has been downloaded from IOPscience. Please scroll down to see the full text.

2014 Nanotechnology 25 025701

(<http://iopscience.iop.org/0957-4484/25/2/025701>)

View [the table of contents for this issue](#), or go to the [journal homepage](#) for more

Download details:

IP Address: 132.216.1.36

This content was downloaded on 13/12/2013 at 16:24

Please note that [terms and conditions apply](#).

One-to-one spatially matched experiment and atomistic simulations of nanometre-scale indentation

D J Oliver¹, W Paul¹, M El Ouali¹, T Hagedorn¹, Y Miyahara¹, Y Qi² and P H Grütter¹

¹ Department of Physics, McGill University, Montreal, QC H3A2T8, Canada

² Department of Chemical Engineering and Materials Science, Michigan State University, East Lansing, 48824, USA


E-mail: oliverd@physics.mcgill.ca

Received 19 July 2013, in final form 6 October 2013

Published 12 December 2013

Abstract

We have carried out nanoindentation studies of gold in which the indenter is atomically characterized by field-ion microscopy and the scale of deformation is sufficiently small to be directly compared with atomistic simulations. We find that many features of the experiment are correctly reproduced by molecular dynamics simulations, in some cases only when an atomically rough indenter rather than a smooth repulsive-potential indenter is used. Heterogeneous nucleation of dislocations is found to take place at surface defect sites. Using input from atomistic simulations, a model of indentation based on stochastic transitions between continuum elastic–plastic states is developed, which accurately predicts the size distributions of plastic ‘pop-in’ events and their dependence on tip geometry.

 Online supplementary data available from stacks.iop.org/Nano/25/025701/mmedia

(Some figures may appear in colour only in the online journal)

1. Introduction

Simulated models that accurately reproduce experimentally observed behaviour are crucial to a number of areas of active research in nanomechanics and nanomaterials. Atomistic simulations are widely used to elucidate mechanisms of plasticity at the nanoscale [1–5], a topic which is relevant to designing nanomechanical devices and to understanding friction and wear at the macroscale. In the realm of new materials discovery, one holy grail is ‘simulation-driven design’, where computer simulations of material behaviour simplify or replace the painstaking trial-and-error task of synthesizing and testing new materials [6, 7]. Empirical atomistic models, such as potential functions, can only be trusted to accurately reproduce material properties if they have been verified against experimental measurements that probe the properties in question. In the case of mechanical properties, the natural experimental technique is nanoindentation.

In the field of nanoindentation, direct comparison between experiment and simulation has been prohibited

by disparities in length and timescales. For simulation, available computational power places an upper bound on these scales; on the experimental side, the limits of instrumental resolution impose a lower bound. Here, thanks to instrumental improvements and the Moore’s law-driven increase in computing power, we are able to close the length-scale gap. Using the technique of field-ion microscopy (FIM) we characterize the indenting tip with atomic precision, allowing us to approach one-to-one atomic correspondence between experimental and model configurations.

On the modelling side, whereas many previous studies have used an idealized, smooth repulsive potential to simulate an indenter tip [2, 8–12], we have chosen to use an atomic tip constructed to match the FIM-imaged experimental tip. This has important consequences. We find that the smooth tip favours homogeneous defect nucleation in the bulk [2], whilst the atomic tip favours heterogeneous nucleation of defects from the tip–substrate interface. The atomic tip also successfully reproduces adhesive effects observed experimentally.

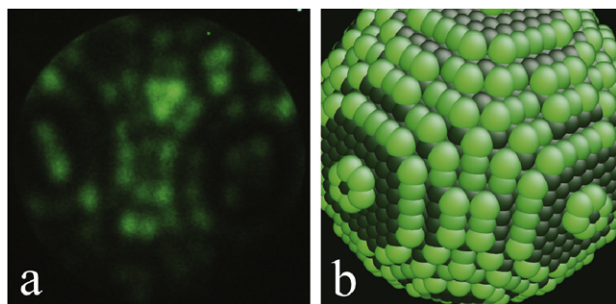


Figure 1. (a) Field-ion microscopy (FIM) image of one of the W(111) tips used. (b) Digital reconstruction of the tip with a radius of 4.1 nm.

We have carried out nanoindentation of gold using extremely sharp tungsten tips with radii of 4–10 nm, recording force–displacement responses and investigating morphology changes by scanning tunnelling microscopy (STM). Molecular dynamics (MD) simulations were carried out to gain qualitative insight into the indentation mechanism.

Finally, we use parameters extracted from atomistic simulations as inputs to a continuum-based stochastic model of indentation, which is able to quantitatively reproduce features of the plastic ‘pop-in’ events observed in the force–displacement curve.

2. Experimental and modelling procedures

All experimental measurements were carried out in a unique custom-built system capable of performing FIM, STM, atomic force microscopy (AFM), and nanoindentation with simultaneous current measurement, all under ultra-high vacuum (UHV) [4, 13–15]. A schematic of the system is shown in the supplementary information (available at stacks.iop.org/Nano/25/025701/mmedia). Single-crystal Au(111) samples were fabricated by depositing 100 nm films of gold on 50 μm -thick mica substrates by thermal evaporation. The mica substrate was mounted as a cantilever and used as a force transducer, by measuring its deflection using optical interferometry [13]. Measurements were performed at cantilever stiffnesses of 100–200 N m^{-1} to avoid jump-to-contact instabilities. The gold surface was treated with several cycles of ion sputtering and annealing in UHV to obtain large 111-oriented terraces free of contamination, as verified by Auger electron spectroscopy. Single-crystal W(111) tips for indentation were prepared by electrochemical etching, then annealed in vacuum to remove residual oxides [16].

FIM was used to atomically characterize the indenter tips. Highly pure He gas was leaked into the measurement chamber, and a high voltage (4–10 kV, depending on tip radius) applied to the tungsten. Due to curvature, the electric field is highest at atom sites at the very end of the tip. He atoms are ionized at these sites and accelerated towards an imaging screen, generating a direct, real-space image of the apex atomic structure, as shown in figure 1.

STM imaging was performed in constant-current mode. Indentations were carried out by retracting the tip 2.5 nm

from the tunnelling contact setpoint (100 pA at 50 mV), approaching the tip to a nominated extension of the piezoelectric tube by continuously ramping the piezo-voltage, and finally retracting to 2.5 nm above the setpoint height, with an approach and retraction duration of 1 s each. The voltage across the junction was maintained at 50 mV during indentation. In a separate study, it was found that bias voltages below 0.12 V had no noticeable effect on mechanical behaviour [17]. Tip–sample rigid-body displacement was determined by subtracting the deflection of the sample cantilever from the extension of the piezoelectric scanner. To minimize interactions, indentations were separated by at least 10 nm. Current was recorded over a pA–mA range, using a logarithmic current-to-voltage converter [18].

The Oliver–Pharr method was used to obtain hardness and modulus values from force–displacement data [19]. For the analysis, the point of contact was taken to be the point of onset of a repulsive force of 7 nN. A spheroconical tip function was used to provide the area function, with the tip radius obtained from FIM images and cone full-angle determined by scanning electron microscopy (SEM) [14]. ‘Pop-ins’ (force–displacement discontinuities) were extracted from the data by taking the differences of successive force values, summing together consecutive differences of the same sign, and thresholding the result.

MD simulations were performed with the LAMMPS software package [20]. The embedded atom method (EAM) was used [21], with a hybridized potential used to describe Au–W interactions, as described in [22]. Dynamics were evaluated by the velocity Verlet method with a timestep of 1 fs. System temperature was maintained at 300 K using the Nose–Hoover thermostat [23]. The indented substrate was a gold slab with xyz dimensions of 24.93 nm \times 25.1 nm \times 11 nm, periodic in the x and y directions, with an upper 111-oriented free surface and a 0.5 nm-thick lower boundary layer of fixed atoms in the z direction. Two different indenter models were used. One indenter was constructed from tungsten atoms, with an atomic structure matched to that of the tip used in experiments. The other indenter was a smooth repulsive force-field with equivalent radius to the real tip. The repulsive potential produces a force on each atom of $F(r) = -K(r - R)^2$, $r < R$, and $F(r) = 0$, $r > R$, where R is the radius of the indenter, r is the distance of the atom from the centre of the indenter, and $K = 16 \text{ nN } \text{\AA}^{-2}$. For each indenter, the indentation method was the same: after an initial wait to allow the system to equilibrate, indentation was performed in a displacement-controlled, stepwise fashion. The tip was approached in 0.025 nm steps with a duration of 2.5 ps, alternated with a 5 ps hold to allow the system to reequilibrate. Simulated force–displacement curves were obtained. Forces were filtered with a lowpass filter in order to suppress thermal vibrational noise and see quasistatic changes more clearly. Defect configurations were visualized by the centrosymmetry parameter (CSP) [2] with the AtomEye program [24]. To calculate pressure for simulations with the W tip, contact area was extracted by dividing the configuration into 1 $\text{\AA} \times 1 \text{\AA} \times 1 \text{\AA}$ voxels which were tested for atomic

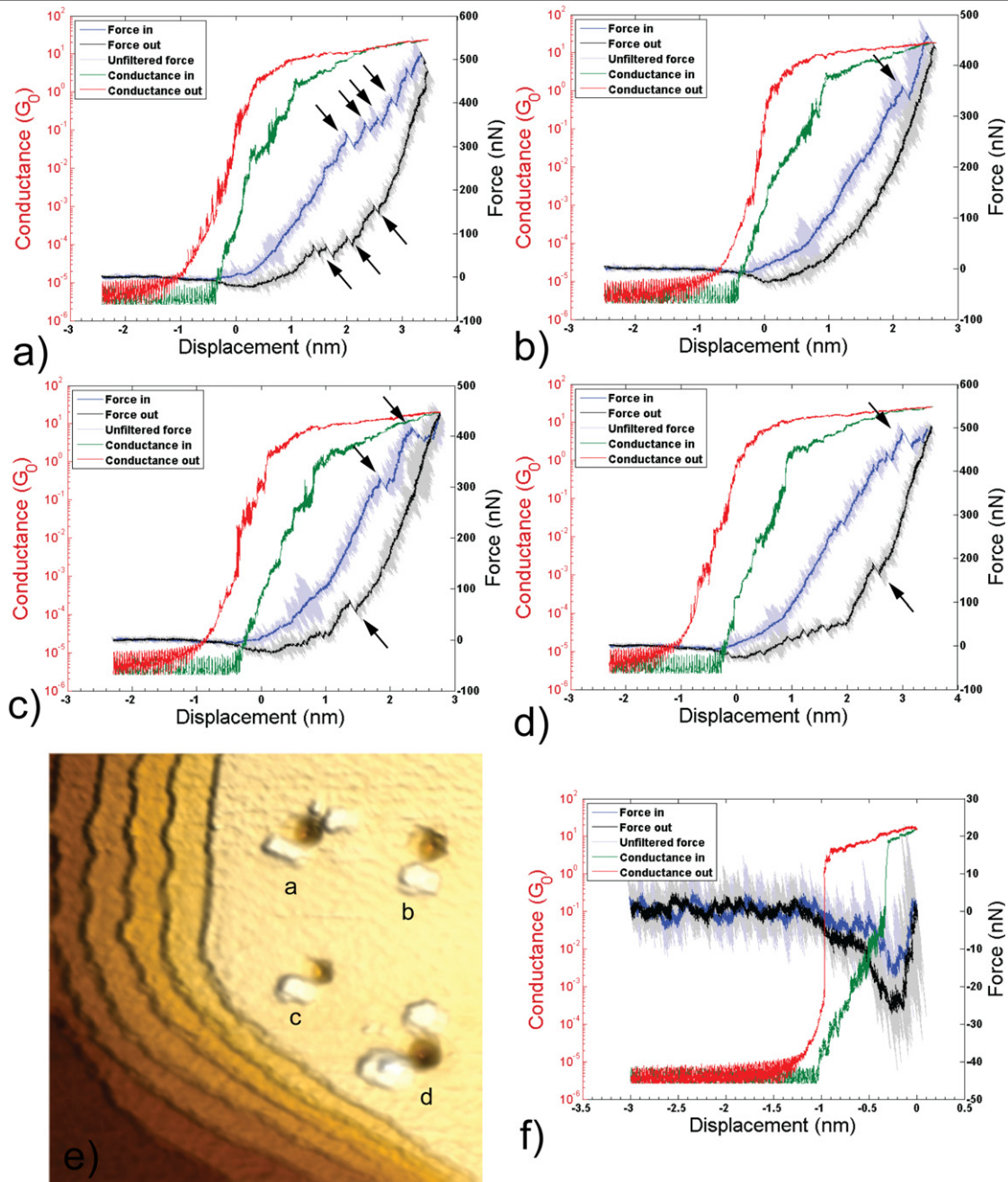


Figure 2. (a)–(d) Typical force–displacement and current–displacement responses (4.1 nm tip). Pop-in and pop-out events are indicated by arrows. For these curves and in the rest of the paper, blue and black lines are (filtered) force on approach and retraction respectively, light-coloured lines are unfiltered force, and green and red lines are conductance on approach and retraction respectively. (e) 100 nm \times 100 nm STM topography scan showing residual impressions corresponding to the presented curves (imaging conditions: 100 pA, 50 mV). (f) Force–displacement curve for an approach just to the onset point of repulsive force.

occupancy assuming an atomic radius of 1.91 Å. The contact area then corresponded to the x – y voxel area at the z -depth of contact between W and Au, or equivalently the minimum x – y voxel area in the configuration.

3. Results

3.1. Experimental results

Figure 2 shows a sample of force–displacement curves from indentations into gold with a 4.1 nm-radius tip, along

with current–displacement curves. Several salient features are apparent. Numerous discrete displacement bursts, or ‘pop-ins’, are visible in each curve on loading. Pop-ins are commonly observed in indentation force–displacement curves and often ascribed to discrete plastic events occurring during loading [3, 4, 12, 25, 26]. Many curves also exhibit reverse displacement bursts, ‘pop-outs’, on unloading. We speculate they may be associated with the annihilation of plastic damage as stress is relieved [4].

A distinctive feature of nanoscale contact between clean metal surfaces is adhesion, in this case between

the gold surface and tungsten tip. This is visible in the force–displacement curve as a region of negative force close to contact on unloading, more clearly seen in the low maximum-load indent in figure 2(f). The hysteresis between the loading and unloading traces in figure 2(f) indicates that energy is dissipated in the contact, suggesting that atomic rearrangements are induced by adhesion. In fact, it can be deduced from the current–displacement curves in figure 2 that at higher loads, a gold wire is drawn out by adhesion as the tip is pulled away from the surface [27, 28]. On unloading the conductance goes to zero, indicating that contact has been broken, ~ 0.5 – 1 nm above the initial free surface as indicated by the point of conduction onset on loading. The opposite would be observed for a Hertzian contact with no adhesion: contact separation and loss of conductance would occur at a depth commensurate with plastic damage.

The STM image in figure 2(e) shows the impressions left in the surface, which are adjoined by material pile-up lobes. These lobes are 1–2 atomic terraces high, and in some cases appear to be hexagonally shaped, corresponding to the threefold symmetry of the 111 surface.

Hardness and elastic modulus were extracted from indents made with a 4.1 nm-radius tip. The reduced elastic modulus was ~ 60 GPa, close to the expected value of ~ 79 GPa [29, 30]. The measured hardness of 10–15 GPa, conversely, is higher than that measured at macroscopic scales by more than an order of magnitude [31]. This is consistent with ‘size effects’ previously observed to affect hardness for indents approaching the nanometre scale [1, 2, 4, 5, 12, 29, 32]. We note that the Oliver–Pharr hardness is likely to be an overestimate because it fails to take into account an increased contact area due to material pile-up [33, 34]. Indeed, hardnesses calculated from directly measuring the contact area from figure 2(e) were found to be 7–10 GPa, comparable to but slightly lower than the hardnesses obtained from the Oliver–Pharr analysis.

Force–displacement pop-in events were collectively extracted and analysed, as described in the method. Datasets for two different tips having radii of 4.1 and 9.5 nm are shown in figures 3(a) and (b) respectively. Each point represents a single pop-in, with the size of the change in force plotted against the onset force. Several features are apparent. Pop-in sizes vary considerably at all onset loads. There is no clear lower bound to the pop-in magnitude: at all onset loads, pop-ins merge continuously with the base instrumental noise in this experimental run (~ 7 nN). There is, however, a clear upper bound to the pop-in magnitude which appears to be an increasing function of the onset force for both datasets. (The two anomalous datapoints in figure 3(b) both come from the same curve, shown in the supplementary information (available at stacks.iop.org/Nano/25/025701/mmedia); we speculate this indent may have been over an imperfection in the sample.) Finally, the upper bound is significantly greater for the sharper tip (figure 3(a)). To explain this trend, we will derive a model which draws from both continuum mechanics theory and atomistic simulations.

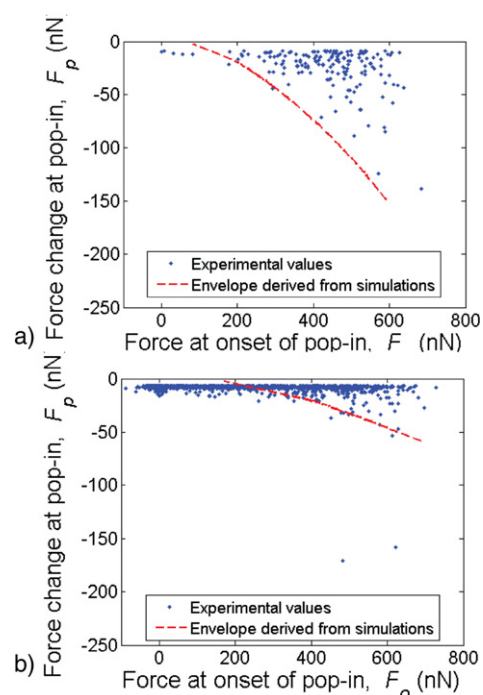


Figure 3. Force change at pop-in plotted versus pop-in onset force, (a) 4.1 nm tip and (b) 9.5 nm tip. Each point represents a pop-in extracted from an experimental curve; the dashed lines are upper-bound envelopes extracted from a continuum-based stochastic model.

3.2. Atomistic modelling results

In order to understand the plastic processes taking place at an atomic scale, molecular dynamics simulations were carried out. Two different methods were used to simulate indentation. Gold was indented with a spherical tip made of tungsten atoms, constructed to match the experimental tip structure of the 4.1 nm-radius tip as determined by FIM. A number of MD studies on gold nanoindentation have used a repulsive spherical ‘bubble’ potential to approximate a real tip [2, 8–12]. To put our results in context with these previous studies, we also ran simulations using a bubble potential with the same radius as the tungsten tip.

Figure 4 shows representative force–displacement curves for indents to ~ 2.3 nm depth. Pop-ins are observed at higher loads, and maximum repulsive loads are comparable for both types of indenter, and also comparable to experimental loads at similar depths (figure 2). For the tungsten-atom tip, a large adhesive (negative-force) region is apparent, particularly in the unloading curve; none is observed for the purely repulsive bubble indenter. We note, however, that the peak adhesive force on unloading is much greater than observed experimentally, 250 nN, as compared to typical experimental values of 50–100 nN.

The points on the force–displacement curves corresponding to onset of plasticity and nucleation of the first dislocation loop are indicated in figure 4. For both tip types, a pop-in is observed, but much more pronouncedly for the bubble indenter. For the rough atomic tip, partial dislocations appear to nucleate from the 2–3 atoms deep layer of disordered atoms

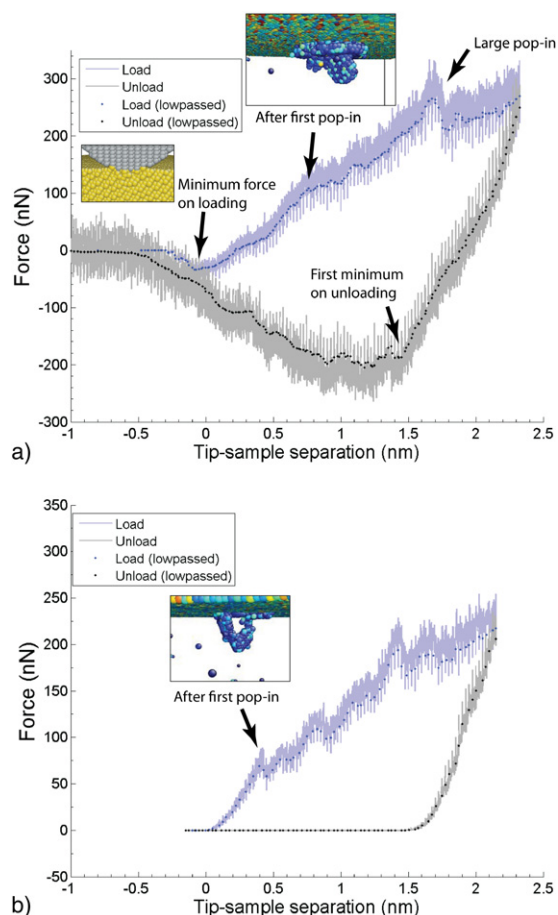


Figure 4. Force–displacement curves extracted from MD simulations: (a) 4.1 nm tungsten-atom tip, (b) 4.1 nm repulsive-potential tip. Insets: subsurface atomic configurations at different stages of the load cycle.

just beneath the tip and extend into the bulk, leaving a planar region of stacking-faulted material (figure 4(a) inset). The disordered layer is seemingly created by conformation of the surface gold atoms to the bcc tungsten tip, causing a registry mismatch with the underlying fcc material. Conversely, for the bubble indenter, a perfect dislocation loop appears to nucleate below the surface, whilst the surface crystal structure is still visibly perfect. The dislocation grows to form a half-loop intersecting the surface (figure 4(b) inset). Taken together, these observations suggest a role of heterogeneous defect nucleation at the tungsten–gold interface in the case of the atomic indenter, and homogeneous nucleation in the bulk for the case of the repulsive-potential indenter, which we will expand upon in the discussion.

An interesting observation for the tungsten-atom tip was that at the point of minimum force on loading, full mechanical contact had already been achieved between the tip and surface. This was confirmed by withdrawing the tip from that point and observing that some gold atoms remained adhered to it.

Pressure versus displacement is shown for the atomic tip in figure 5. The pressure initially increases sharply, until plateauing at a point roughly corresponding to the nucleation of the first dislocation, at a level of ~ 5 GPa. Later, prior to the

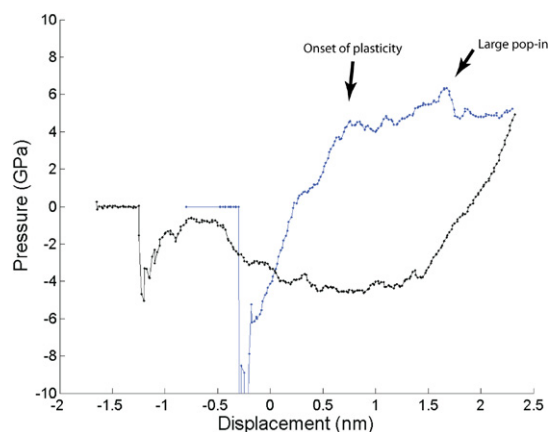


Figure 5. Contact pressure versus displacement, extracted from MD simulation with a 4.1 nm tungsten-atom tip.

large pop-in visible in figure 4(a), the pressure ‘overloads’ to ~ 6.4 GPa, dropping back after the pop-in to previous levels.

Defect configurations at maximum load are shown in figures 6(a) and (b), visualized by centrosymmetry parameter (degree of local deviation from crystalline symmetry) [2]. Atoms with perfect crystalline symmetry are hidden. Plastic damage consists of a number of stacking-fault ribbons lying on close-packed (111) planes, sandwiched between $[112]/6$ partial dislocations.

During unloading, much of the induced plastic damage in the gold substrate spontaneously anneals out. In the case of the tungsten-atom tip, it is replaced by an inverted-pyramid (111) stacking-fault structure, observable in figure 6(c), which forms at the point of the first load minimum marked in figure 4(a). (A similar, smaller inverted-pyramid briefly forms during the negative-force period on loading.) On retraction a gold wire is drawn out between the tungsten tip and gold surface, a remnant of which is visible in the centre of the impression where it was anchored (figure 6(e)), and can be seen more clearly in the movie provided in the supplementary information (available at stacks.iop.org/Nano/25/025701/mmedia).

Whilst the profile of the indent formed by the bubble indenter is roughly regular hexagonal (figure 6(f)), the indent left by the tungsten-atom tip has a truncated-triangular profile, seen more clearly in figure 7(a). The edges of the triangle align with the inverted-pyramid defect structure on 111 planes that is visible in figure 6(c). Interestingly, a similar truncated-triangle profile has been experimentally observed in high-resolution STM images acquired immediately after indentation; an example is shown in figure 7(b).

3.3. Simulated indentation using a continuum-based model of stochastic state transitions

Although it is possible, as we have demonstrated, to carry out atomistic simulations matching experimental nanoindentation, it is still computationally prohibitive to carry out more than a few such simulations. (The configuration in figure 6 represents roughly 800 CPU h of computations.) Thus it is not possible to compare MD results with experimental

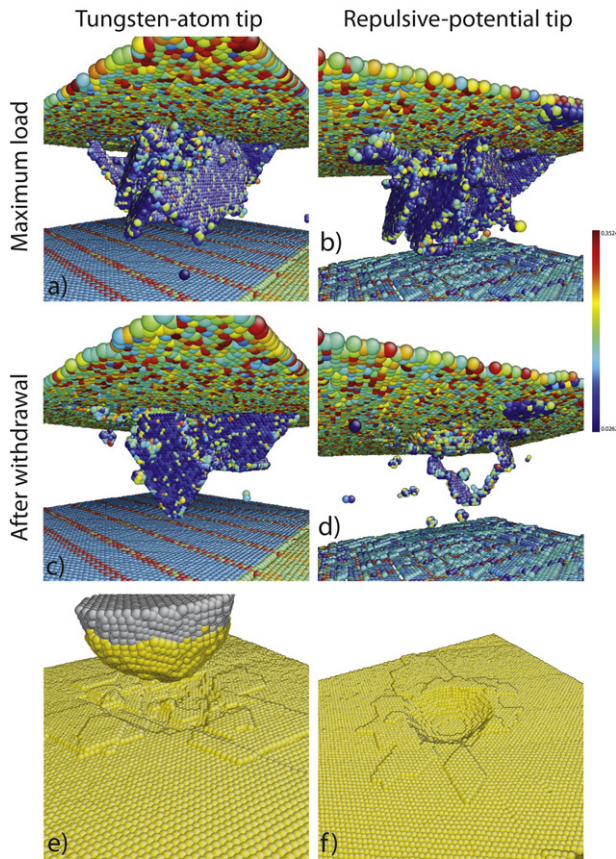


Figure 6. MD visualizations for tungsten-atom tip ((a), (c), (e)) and repulsive-potential tip ((b), (d), (f)). In (a)–(d) atoms are coloured by centrosymmetry parameter (CSP), and only atoms with increased CSP (i.e., at defects) are shown. In (e) and (f) atoms are coloured by element type. (a), (b) Defect configurations at maximum indentation load. (c), (d) Defect configurations after indenter withdrawal. (e), (f) Surface deformation after indenter withdrawal.

results only observed over a large ensemble of indents, such as the distribution of pop-ins shown in figure 3. In order to fill this gap, we have developed a much more tractable model of plastic indentation based upon continuum mechanics.

Previous classical models of nanoindentation have either employed a quasistatic assumption, under which plastic deformation is steady, continuous, and deterministic [19, 35], or have utilized numerical finite-element methods [33, 36]. In order to reproduce the discontinuous pop-in behaviour characteristic of experimental results without necessitating the full machinery of finite-element modelling, we have developed a stochastic model of indentation, in which plasticity is permitted to occur in discrete, abrupt bursts, due to ‘overloading’ above the steady-state yield stress of the material.

The model is as follows. For simplicity, we assume that the indenter–substrate system can be in one of only two states. In the first state, the substrate is undergoing continuous-plastic flow; both elastic and plastic displacements occur as load is increased. In the second state, plastic flow is arrested (as, for instance, due to pinning of interlocking dislocations) and only elastic displacements take place. In the first state, contact pressure and maximum shear stress remain constant as load is

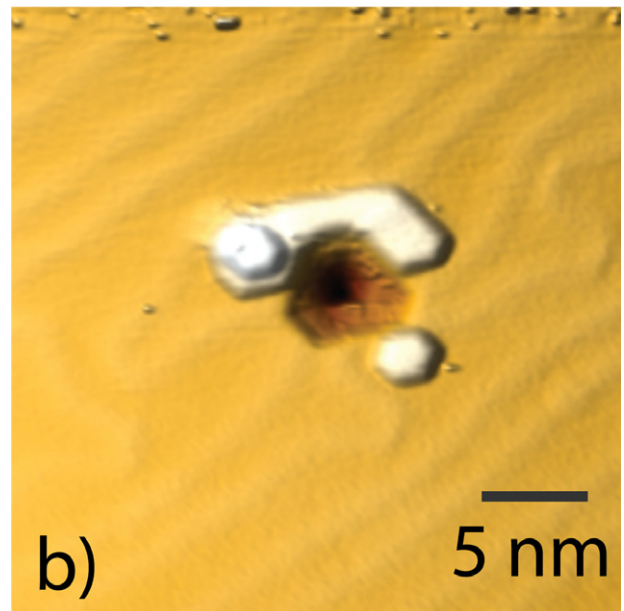
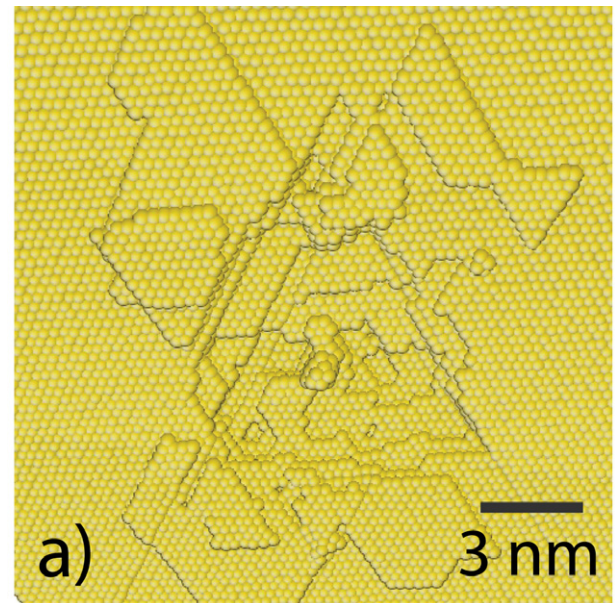


Figure 7. (a) Surface profile of tungsten-atom MD indent. (b) 3d rendering of an experimental topographic STM image of an indent in gold (imaging conditions: 9 pA, −0.9 V). The gold surface’s herringbone reconstruction ridges have rearranged in the vicinity of the indentation to accommodate changes in surface stress.

increased. In the second state, stresses continually increase. The second state also describes initial elastic deformation prior to any plasticity. The equations of the elastic–plastic state for a spherical tip have been described by Field and Swain [35]. Displacement and contact radius as functions of force are given by:

$$a = a_c \sqrt{F/F_c} \quad (1)$$

$$d = R - \sqrt{R^2 - a^2} + \frac{3}{8} \frac{F}{E^* a} \quad (2)$$

where F is the force, a is the contact radius, d is the displacement, E^* is the reduced elastic modulus, R is the tip

radius, and F_c and a_c are the critical force and contact radius at which plasticity is initiated, that is, at which the elastic contact pressure reaches the hardness of the material.

The elastic state is simply described by the Hertzian equation [37] with an effective tip radius and an offset determined by the amount of plastic deformation already accumulated (or equal to the tip radius in the initial damage-free state):

$$a = \left(\frac{3FR^*}{4E^*} \right)^{1/3} \quad (3)$$

$$d = d_i + \frac{a^2 - a_i^2}{R^*} \quad (4)$$

$$R^* = \begin{cases} \frac{4E^*a_i^3}{3F_i}, & \text{if } F_i > 0 \\ R, & \text{if } F_i = 0 \end{cases} \quad (5)$$

where R^* is the effective tip radius and F_i , d_i , and a_i are the initial force, displacement, and contact radius at the commencement of the state.

Stochasticity is introduced via the transition rules from one state to the other. Transition from the plastic state to the elastic state is allowed to occur with a fixed probability on each force increment. From the elastic state, transition occurs at an ‘overload stress’ selected from within a nominated range with a linear probability distribution function (maximum probability at an overload ratio of 1, approaching to zero probability at the maximum possible overload ratio). This distribution shape was arbitrarily selected to reproduce the empirical observation that more smaller pop-ins are observed than larger pop-ins. The maximum overload ratio was extracted from MD simulation, by taking the ratio of the maximum contact pressure in figure 5 of ~ 6.4 GPa, to the post-pop-in contact pressure of ~ 4.8 GPa, giving a ratio of 1.3. When the elastic state transitions to the plastic, a pop-in occurs, with a slope (dP/dh) determined by the experimental spring constant of the system (the cantilever spring constant). These states are shown in figure 8(a) (inset).

Using equations (1)–(5) and the transition rules described, we can numerically simulate an entire force–displacement loading curve. Some examples are shown in figure 8. A large number of indents were simulated for both the 4.1 nm tip and the 9.5 nm tip using Matlab, in both cases using experimentally measured parameters as inputs to the model (hardness, elastic modulus, cantilever spring constant, and tip radius). Statistics of pop-ins were extracted from simulated curves. The results, presented in figure 9, show good agreement with the data in figure 3. Envelope curves, obtained by setting the elastic-to-plastic transition stress to a fixed ratio of 1.3, are plotted in figure 3 showing the maximum pop-in size at a given onset load predicted by the model. The envelope curves are in excellent quantitative agreement with the data, and correctly reproduce the inverse proportionality of maximum pop-in size to tip radius.

Several of the stochastic parameters of the model were systematically varied to investigate their importance. Varying the probability of a transition out of the plastic state causes

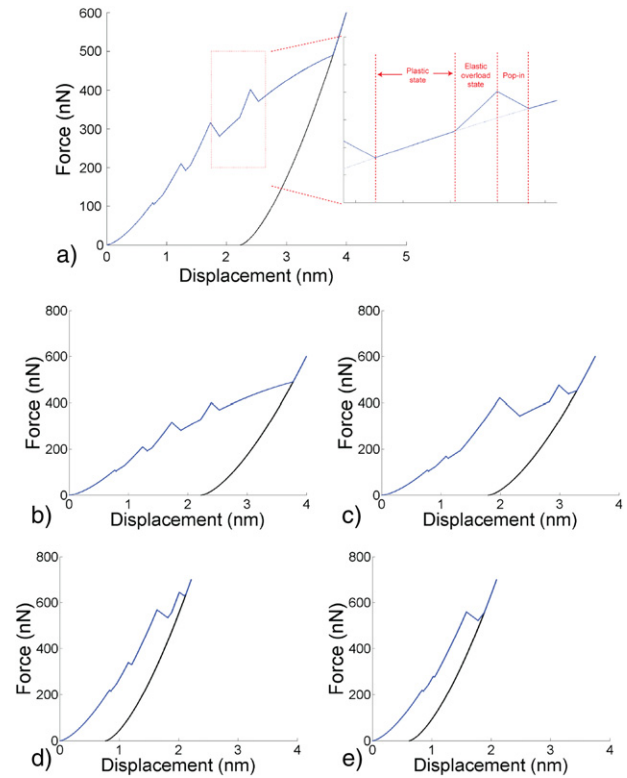


Figure 8. (a) Simulated force–displacement curve, with zoomed inset showing states involved in the calculation. (b), (c) Simulated curves for 4.1 nm tip. (d), (e) Simulated curves for 9.5 nm tip.

the number of pop-ins per curve to change, but does not affect their statistical size distribution. Varying the probability distribution function of the overload stress for the transition out of the elastic state causes the statistical distribution of the pop-ins to change, but does not affect the maximum pop-in size. The maximum pop-in size is affected by the maximum overload ratio, but for plausible values it appears to be relatively insensitive to this parameter: setting the maximum overload ratio to 1.1 and 1.7 changed the maximum pop-in size by about -40% and $+10\%$ respectively, relative to an overload ratio of 1.3. A very large set of indentation curves would be required to obtain the statistical power needed to experimentally determine the maximum overload ratio with better precision.

4. Discussion

Numerous points of similarity are observed between simulation and experiment, including pop-ins, adhesion, wire-pulling, material pile-up, and indent morphology. We find it striking that the same truncated-triangular profile is observed both for MD and experimental indents. In the MD case, the triangular shape appears to be caused by the formation of an inverted-pyramid stacking-fault structure underneath the indenter, which forms under adhesion-induced tensile stress, after compression-induced defects have spontaneously annealed out. The similarity is evidence that similar atomistic processes are taking place.

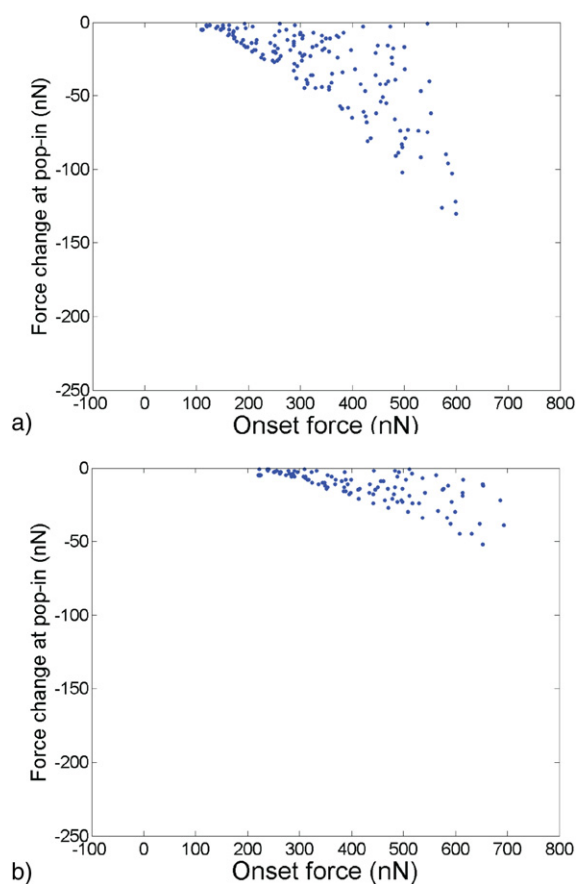


Figure 9. Force change at pop-in versus pop-in onset force, each point representing a pop-in extracted from simulated indentation runs. (a) 4.1 nm tip and (b) 9.5 nm tip.

For simulations with the atomic tip, a single layer of gold adheres to the tip upon retraction. This implies that Au–W bonds are stronger than Au–Au bonds for the potential used, which was confirmed by carrying out static simulations of an Au–W interface and extracting potential energies (see suppl. inf. available at stacks.iop.org/Nano/25/025701/mmedia). The removal of the adhered layer of Au contributes to the residual impression in the surface. In these simulations this is a significant contribution, because all dislocations formed on loading are annihilated during unloading.

Simulations were carried out with both a tungsten-atom tip matched to the 4.1 nm experimental tip, and a 4.1 nm repulsive-potential ‘bubble’ indenter as used in several previous studies. The most noteworthy difference, apart from the absence of adhesion-related phenomena for the bubble indenter, was the apparently different modes of dislocation nucleation. The roughness of the atomic tip induces conformational defects at the tungsten–gold interface, providing reduced-energy nucleation sites. Additionally, the very sharp radius (4.1 nm) of the tip localizes shear stresses very close to the surface. In combination, these effects appear to lead to heterogeneous nucleation at surface defects being favoured. For the smooth bubble indenter, it appears that instead homogeneous dislocation nucleation is favoured. These observations are consistent with a previous modelling

study by Wagner *et al* on aluminum, who also observed that atomically rough tips could supply surface nucleation sites that were absent for smooth tips [38]. Since real tips are atomically rough, we would expect heterogeneous nucleation to occur for comparable experimental conditions. This is supported by recent evidence from experimentally observed first pop-in loads for heterogeneous nucleation in the same material system [15].

We note that the quantitative agreement between experiment and MD simulation is imperfect; the simulation significantly overestimates the magnitude of the adhesive pull-off force. This was also true for simulations (not shown) in which a tungsten tip wetted with gold was indented into a pristine surface. We note that maximum adhesive forces given by the JKR and DMT models for this tip are <100 nN, much less than observed in the MD; this is consistent with the fact that JKR and DMT are essentially elastic models, whereas the pull-off process in the MD simulation involves inelastic material rearrangements, which act to increase the adhesive contact area. Although we have closed the length-scale gap, there is still a 9-orders of magnitude disparity in timescales, which precludes the observation of certain dynamics. It is possible, for example, that diffusive rearrangements on timescales much larger than picoseconds act to reorder the contact to minimize the pull-off force. Conventional MD is limited by the need for the timestep to be much smaller than the smallest characteristic timescale of the system (typically atomic vibration). Several approaches have been developed to try to extend MD to long timescales, including kinetic Monte Carlo methods [39] and diffusive molecular dynamics [40]. All of these methods have particular strengths and weaknesses. Pursuit of such models is imperative to be able to carry out a truly robust comparison between simulation and experiment.

The observation in MD of mechanical tip–substrate contact at measured net negative loads warrants further comment. Although it is initially surprising, it can be easily explained: the contact area, where atomic interactions are repulsive, is surrounded by an annulus (as per the DMT model [41]) in which non-contacting tip and surface atoms exert a mutual attractive force. Clearly, whilst the area of direct contact is small, the non-contact annulus will have a larger contact area, and a net negative force can be obtained. This is consistent with, e.g., the previous study of nickel–gold contact by Landman *et al* [1]. This is an important consideration for scanning probe microscopy studies, particularly non-contact atomic force microscopy (NC-AFM). NC-AFM is typically conducted in the attractive force regime to minimize tip–sample interactions, but since only the net force is measured, the apex of the tip may be in mechanical contact with the sample, potentially resulting in material transfer or tip damage.

We have developed a preliminary indentation model based upon stochastic transitions between continuum-mechanical states which captures aspects of pop-in behaviour. The stochastic quality of the model is consistent with our previous experimental observations that plastic yield load varies considerably between individual indents [15]. It is

uncertain whether this variance is due to preexisting defects in the material, or due to the thermally induced character of heterogeneous nucleation. Some phenomena have not been considered in the model in the interest of simplicity. Thermal activation frequently plays an important role in indentation-induced plasticity [26, 42]. Thermal activation would introduce a loading-rate dependence of the maximum pop-in size: higher loading rates reduce the number of 'attempts' to initiate or move a plastic defect, thereby allowing larger pop-ins to occur (equivalent to increasing the overload stress ratio in the model). Another question that can be asked is whether the continuous-plastic state used in the model has any actual validity, or whether all plastic deformation during indentation is discontinuous to some degree. It is difficult to definitively answer this question experimentally because small pop-ins may simply be masked by experimental noise (we have previously observed pop-ins as small as 1 nN [15]), but a closer analysis of the model might reveal statistical differences between the two cases which can be compared with experiment.

5. Conclusion

In summary, we have carried out experimental tungsten-on-gold nanoindentation studies, and performed one-to-one spatially matched simulations using molecular dynamics. Numerous features of experiment are reproduced in simulation, including wire-drawing, material pile-up, and morphology of the residual impression. Comparison of a simulated tungsten-atom tip and a repulsive-potential tip shows that the atomic tip more closely matches qualitative experimental observations. 'Pop-in' events are observed in both experiment and simulation, and are found to correspond to the nucleation of dislocations on close-packed (111) planes. This nucleation is heterogeneous in the case of a sharp, atomically rough tip. Finally, we have developed a continuum-based stochastic model of indentation which, using parameters obtained from simulation and experiment, accurately describes the envelope of pop-in magnitudes observed experimentally.

Acknowledgments

Funding for this research was provided by the Natural Sciences and Engineering Council of Canada, including a Vanier Scholarship, and the Fonds Québécois de la Recherche sur la Nature et les Technologies.

References

- [1] Landman U, Luedtke W D, Burnham N A and Colton R J 1990 *Science* **248** 454
- [2] Kelchner C L, Plimpton S J and Hamilton J C 1998 *Phys. Rev. B* **58** 11085
- [3] Van Vliet K J, Li J, Zhu T, Yip S and Suresh S 2003 *Phys. Rev. B* **67** 104105
- [4] Cross G L W, Schirmeisen A, Grutter P and Durig U T 2006 *Nature Mater.* **5** 370
- [5] Ward D K, Farkas D, Lian J, Curtin W A, Wang J, Kim K S and Qi Y 2009 *Proc. Natl Acad. Sci.* **106** 9580
- [6] Olson G B 2000 *Science* **288** 993
- [7] Lewis A C, Bingert J F, Rowenhorst D J, Gupta A, Geltmacher A B and Spanos G 2006 *Mater. Sci. Eng. A* **418** 11
- [8] Zimmerman J A, Kelchner C L, Klein P A, Hamilton J C and Foiles S M 2001 *Phys. Rev. Lett.* **87** 165507
- [9] Rodríguez de la Fuente O, Zimmerman J A, González M A, de la Figuera J, Hamilton J C, Pai W W and Rojo J M 2002 *Phys. Rev. Lett.* **88** 036101
- [10] Knap J and Ortiz M 2003 *Phys. Rev. Lett.* **90** 226102
- [11] Lilleodden E T, Zimmerman J A, Foiles S M and Nix W D 2003 *J. Mech. Phys. Solids* **51** 901
- [12] Navarro V, Rodríguez de la Fuente O, Mascaraque A and Rojo J M 2008 *Phys. Rev. Lett.* **100** 105504
- [13] El Ouali M 2010 *PhD Thesis* McGill University
- [14] Oliver D J, Maassen J, El Ouali M, Paul W, Hagedorn T, Miyahara Y, Qi Y, Guo H and Grütter P 2012 *Proc. Natl Acad. Sci.* **109** 19097–102
- [15] Paul W, Oliver D, Miyahara Y and Grütter P H 2013 *Phys. Rev. Lett.* **110** 135506
- [16] Hagedorn T, El Ouali M, Paul W, Oliver D, Miyahara Y and Grutter P 2011 *Rev. Sci. Instrum.* **82** 113903
- [17] Paul W 2013 *PhD Thesis* McGill University
- [18] Dürig U, Novotny L, Michel B and Stalder A 1997 *Rev. Sci. Instrum.* **68** 3814
- [19] Oliver W and Pharr G 1992 *J. Mater. Res.* **7** 1564
- [20] Plimpton S 1995 *J. Comput. Phys.* **117** 1
- [21] Daw M S, Foiles S M and Baskes M I 1993 *Mater. Sci. Rep.* **9** 251
- [22] Zhou X W, Johnson R A and Wadley H N G 2004 *Phys. Rev. B* **69** 144113
- [23] Hoover W G 1985 *Phys. Rev. A* **31** 1695
- [24] Li J 2003 *Modelling Simul. Mater. Sci. Eng.* **11** 173
- [25] Lorenz D, Zeckzer A, Hilpert U, Grau P, Johansen H and Leipner H S 2003 *Phys. Rev. B* **67** 172101
- [26] Schuh C A, Mason J K and Lund A C 2005 *Nature Mater.* **4** 617
- [27] Agraït N 2003 *Phys. Rep.* **377** 81
- [28] Kizuka T 2008 *Phys. Rev. B* **77** 155401
- [29] Kiely J D and Houston J E 1998 *Phys. Rev. B* **57** 12588
- [30] 2011 *CRC Handbook of Chemistry and Physics* 92nd edn (Boca Raton, FL: CRC Press LLC)
- [31] Nix W D, Greer J R, Feng G and Lilleodden E T 2007 *Thin Solid Films* **515** 3152
- [32] Sutton A P and Pethica J B 1990 *J. Phys.: Condens. Matter* **2** 5317
- [33] Bolshakov A and Pharr G M 1998 *J. Mater. Res.* **13** 1049
- [34] Oliver W and Pharr G 2004 *J. Mater. Res.* **19** 3
- [35] Field J S and Swain M V 1993 *J. Mater. Res.* **8** 297
- [36] Begley M R and Hutchinson J W 1998 *J. Mech. Phys. Solids* **46** 2049
- [37] Johnson K 1985 *Contact Mechanics* (Cambridge: Cambridge University Press)
- [38] Wagner R J, Ma L, Tavazza F and Levine L E 2008 *J. Appl. Phys.* **104** 114311
- [39] Henkelman G and Jonsson H 2001 *J. Chem. Phys.* **115** 9657
- [40] Li J, Sarkar S, Cox W T, Lenosky T J, Bitzek E and Wang Y 2011 *Phys. Rev. B* **84** 054103
- [41] Derjaguin B V, Muller V M and Toporov Y P 1975 *J. Colloid Interface Sci.* **53** 314
- [42] Schuh C A and Lund A C 2004 *J. Mater. Res.* **19** 2152